Jurnal Elektronika dan Telekomunikasi (JET), Vol. 23, No. 1, August 2023, pp. 9-15
Accredited by KEMDIKBUDRISTEK, Decree No: **158/E/KPT/2021**
doi: 10.55981/jet.537

Dual-band Via-less Band-pass Filter Based on Cascaded Closed Ring Resonator

Teguh Firmansyah[a, *], Supriyanto Praptodiyono[a], Achmad Rifai[a], Syah Alam[b], Ken Paramayudha[c]

[a] Department of Electrical Engineering
Universitas Sultan Ageng Tirtayasa
Jl. Jenderal Sudirman Km 3, Kotabumi, Kec. Purwakarta
Cilegon, Indonesia
[b] Department of Electrical Engineering
Universitas Trisakti.
Jl. Letjen S. Parman No.1, Grogol
Jakarta, Indonesia
[c]Research Center for Telecommunication
National Research and Innovation Agency, Indonesia (BRIN)
Jl. Sangkuriang, Dago
Bandung, Indonesia

Abstract

A band-pass filter (BPF) is an essential part of a wireless communication system as it functions to reduce interference and noise. Many structures have been proposed to achieve a high-quality BPF. Typically, these structures utilize vias. However, vias has several drawbacks, including impedance discontinuities, increased resistance values, and complex structures. In this study, we propose a dual-band BPF based on a cascaded closed ring resonator (CCRR) without using vias. Specifically, the proposed structure consists of multiple CCRRs connected at the corner pattern and incorporates capacitive coupling to the input impedance. Additionally, the CCRR configuration has dual sizing to achieve dual-band performance. Subsequently, the proposed BPF is simulated and fabricated using Duroid Rogers RT 5880 with dielectric constant $\varepsilon_r = 2.2$, dissipation factor tan $\delta = 0.0009$, and thickness h = 1.575 mm. The measurement results demonstrated that the dual-band BPF operated at a resonant frequency of 2.50 GHz with a transmission coefficient (S_{21}) value of -2.18 dB in the first band. In the second band, a resonant frequency of 3.70 GHz was obtained with an S_{21} value of -1.43 dB. The bandwidth in the first band was 160 MHz, and in the second band, it was 110 MHz. Moreover, based on the measurement results, the reflection coefficient (S_{11}) in the first band was -11.05 dB, while in the second band, it was -23.3 dB. The excellent agreement between the simulation and measurement validates the proposed method.

Keywords: dual-band, band-pass filter, CCRR, via-less.

I. INTRODUCTION

A band-pass filter (BPF) is an important part of the wireless communication system. It has a function for interference and noise reduction. Many structures were proposed to obtain a good quality of BPF [1]–[5]. BPF has several parameters, such as transmission coefficient, reflection coefficient, frequency center, and bandwidth [6]–[9]. There are several interesting methods to develop dual-band BPF. Firmansyah *et al.* [10] proposed dual-wideband BPF. A cross-stub stepped impedance resonator (CS-SIR) was utilized to obtain dual wideband performance. Moreover, the BPF was analyzed using an impedance model. Besides, Aribowo introduced a multi-stub resonator to obtain dual-band BPF. The proposed BPF has a frequency center of 0.9 GHz and 1.85 GHz. The proposed filter structure has a drawback, such as its large size [11]. Therefore, meandering structures [11]–[13] and folding [14] are usually used to reduce the size of BPF.

Weng *et al.* [15] propose dual-band BPF by combining the stepped impedance resonators (SIRs) and multilayered structures. The proposed filter has a wide and narrow band with a frequency center of 2.4 GHz and 5.2 GHz. The proposed BPF has several multipath propagations to produce multi-transmission zeros. Moreover, Chang *et al*. [16] proposed dual-band BPF with hairpin-line resonators and slot-coupled resonators based on a multilayered structure. The proposed filter has a frequency of 2.4 GHz and 5 GHz. Moreover, discriminating coupling is introduced. Therefore, the number of transmission zeros is increasing. The simulation and measurement have a good agreement.

Another interesting method was proposed by Ta *et al.* [17]. The quasi-lumped hybrid LC resonators were proposed. Then, the shunt-inductor impedance inverters were also developed. The proposed resonator structure was developed based on a multilayer organic substrate. Moreover, it had a frequency of 1.7 GHz and 4.0 GHz. The next dual-band BPF research is based on the design of low-temperature co-fired ceramics (LTCC). The LTCC structure was proposed by Elelimy *et al.* [18]. The

* Corresponding Author.
Email: teguhfirmansyah@untirta.ac.id
Received: February 01, 2023 ; Revised: May 29, 2023
Accepted: June 22, 2023 ; Published: August 31, 2023

LTCC is a combination of broadside-coupled and edge-coupled strip lines with a multilayer structure. A multilayered structure is a good strategy for reducing the size of BPF. However, it has several drawbacks, such as complex structure dan unnecessary electromagnetic coupling between layers.

Moreover, Tang *et al.* [19] proposed substrate-integrated defected ground structure (SIDGS) to obtain dual-band BPF with low loss. The structure has two different defective ground structures (DGSs) surrounded by metal vias. The dual-band BPF operates at 2.10 and 3.78 GHz. Then, a substrate integrated waveguide (SIW) filter using dual-complementary split ring resonator (CSRRs) and Z-shaped was proposed by Yin [20]. Utilizing a SIW can increase the flatness in the pass band. Multiple vias are used to obtain the SIW configuration. Furthermore, Iqbal *et al.* [21] introduced a dual-band half-mode SIW filter. A couple of E-shaped coupling slots with half-mode substrate integrated waveguide (HMSIW) were arranged. The proposed BPF has suitable for integration with a planar structure. Then, an ultra-wide BPF using an integrated substrate gap waveguide is proposed by Ruan *et al.* [22]. However, using vias has several drawbacks, such as complex structure, high resistance, expensive, and high possibility of unnecessary mixed signals.

This research proposed dual-band via-less BPF based on a cascaded closed ring resonator. The proposed filter has a single-layered structure. It has a simple structure and is easy to fabricate. Moreover, the via-less configuration can avoid high resistance. In detail, the dual-band BPF is essential for making a more efficient RF device due to concurrent implementation.

Moreover, the ring resonators have several advantages compared to other types of resonators at microwave frequencies, such as highly compact. They can be fabricated on a small chip, making them suitable for integration in miniaturized microwave circuits. Then, the geometry of a ring resonator can be easily modified to tune its resonant frequency. By adjusting the radius or width of the ring, the resonant frequency can be tailored to specific applications or easily adjusted during the design process. Ring resonators generally exhibit low dispersion, allowing them to maintain their resonant frequency over a wide range of input frequencies. It has a planar technology that enables cost-effective mass production and integration with other planar microwave components.

It should be noted that the proposed BPF was designed for WLAN and 4G (2.4 - 2.6 GHz) and upper band 4G (3.5 - 3.7 GHz) applications. Then, the proposed BPF should meet several specifications, such as the transmission coefficient value is better than -3 dB, the reflection coefficient is better than -10 dB, dan the minimum bandwidth is 100 MHz. Finally, this paper is separated into several parts. The second part is investigation the fundamental of ring resonators. Then, it is followed by single-band and dual-band filter optimization and implementation. Moreover, part three is focused on fabrication, measurement, and discussion. Then the last part is the conclusion.

II. Investigation of Close Ring Resonator

Figure 1 shows the fundamental structure of a closed-shape ring resonator with feed line input impedance. Moreover, it has a capacitive coupling with a gap distance of s_1. Then, the input impedance feeding has an impedance value of Z_0 with a width of W_0. The impedance value of the ring resonator is Z_r, with a width of W_r. The proposed ring resonator has a rectangular shape. Moreover, Figure 2 illustrates a simple transmission line model of a closed ring resonator.

In detail, we can determine the impedance of the ring resonator Z_{ring} when the input voltage (V_1), input current (I_1), output voltage (V_2), and output current (I_2) are known, specifically when $I_2 = 0$.

By keeping the V_2 and I_2 open-circuited. The Z_{ring} can be determined by (1).

$$Z_{ring} = \frac{V_1}{I_1}\Big]_{I_2=0.} \quad (1)$$

Moreover, we can approximate the impedance by using ABCD matrix calculation. In detail, the transfer matrix of a single structure of ring resonator can be calculated by (2).

$$\begin{bmatrix} A & B \\ C & D \end{bmatrix} = \begin{bmatrix} \cos\beta l_{1,2} & jZ_r \sin\beta l_{1,2} \\ j\,Y_r \sin\beta l_{1,2} & \cos\beta l_{1,2} \end{bmatrix} \quad (2)$$

where the β is the propagation constant. Then, by using the conversion from the ABCD matrix to Y-matrix. Y-matrix can be calculated as (3).

$$\begin{bmatrix} Y_{11} & Y_{12} \\ Y_{21} & Y_{22} \end{bmatrix} = \begin{bmatrix} -jY_r \cot\beta l_{1,2} & j\,Y_r \csc\beta l_{1,2} \\ j\,Y_r \csc\beta l_{1,2} & -jY_r \cot\beta l_{1,2} \end{bmatrix} \quad (3)$$

Because the ring resonator has a dual structure, such as an upper ring structure and lower ring structure with a length of l_1 represented by the value of d_1 and a length of l_2 represented by the value of d_2. The Y-matric value of the ring resonator can be determined by (4).

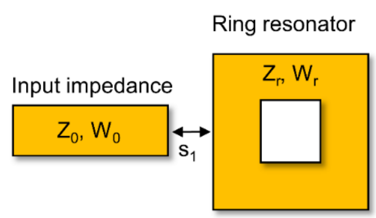

Figure 1. A simple structure of ring resonator with line input impedance with capacitive coupling.

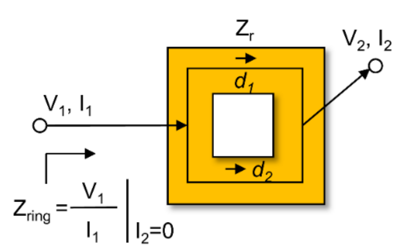

Figure 2. Voltage, current, and impedance approach of a simple structure of ring resonator with line input impedance with capacitive coupling.

$$\begin{bmatrix} Y_{11} & Y_{12} \\ Y_{21} & Y_{22} \end{bmatrix}_{ring} = jY_r \begin{bmatrix} -\cot\beta l_1 & \csc\beta l_1 \\ \csc\beta l_1 & -\cot\beta l_1 \end{bmatrix} + jY_r \begin{bmatrix} -\cot\beta l_2 & \csc\beta l_2 \\ \csc\beta l_2 & -\cot\beta l_2 \end{bmatrix} \quad (4)$$

then, the Y_{ring} can be evaluated by (5).

$$Y_{ring} = \frac{Y_{11}Y_{22} - Y_{12}Y_{21}}{Y_{22}} \quad (5)$$

Moreover, the Z_{ring} can be calculated by (6).

$$Z_{ring} = \frac{Y_{22}}{Y_{11}Y_{22} - Y_{12}Y_{21}} = \frac{P}{Q-R} \quad (6)$$

where $P = -jY_r(\cot\beta l_1 + \cot\beta l_2)$

$$Q = [-jY_r(\cot\beta l_1 + \cot\beta l_2)]^2$$

$$R = [-jY_r(\csc\beta l_1 + \csc\beta l_2)]^2$$

The relation between Z_{ring} value and C_{ring}, and also Z_{IN} and C_{IN} value, are evaluated by (7)-(8).

$$Z_{ring} = \frac{1}{j\omega C_{ring}} \quad (7)$$

$$Z_{IN} = \frac{1}{j\omega C_{IN}} \quad (8)$$

If the parallel capacitance (C_P) and gap capacitance (C_G) are considered. The C_{IN} can be determined by (9).

$$C_{IN} = \frac{C_pC_g + C_pC_{ring} + C_gC_{ring}}{C_g + C_{ring}} \quad (9)$$

Figure 3 shows the relations between C_{ring} and C_{IN} of the proposed ring resonator structure. Here, the parallel capacitance (C_P) and gap capacitance (C_G) are calculated. In detail, the red line shows the effect of the variation of C_G on the total C_{IN} value when the parallel capacitance of C_P is constant. It can be seen that the C_G has a significant effect on the C_{IN} value. Moreover, the blue line shows the variation of C_P to the total C_{IN} value when the parallel capacitance of C_G is slightly constant. It can be seen that the C_{IN} value is almost stable with a little increase at C_P < 3pF. Therefore, we can see that the C_P and C_G have influenced C_{IN} value with different weights. This result also indicated that the gap dan parallel would affect resonance frequency. In detail, the effect of C_{IN} value with change the value of Z_{IN} and its lead to the change of frequency center.

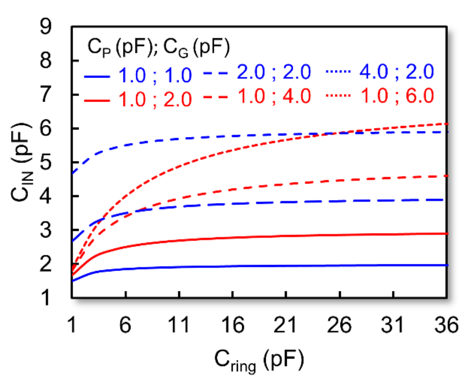

Figure 3. Relations between C_{ring} and C_{IN} of the proposed ring resonator structure, where parallel capacitance (C_P) and gap capacitance (C_G).

III. Single/ Dual Band Via-Less Microstrip Band-pass Filter Based on Multistructure Close Ring Resonators

Figure 4 shows a structure of a single band via-less microstrip band-pass filter based on close ring resonators. It can be seen that the ring resonator has an outer dimension of W_1 and an inner dimension of W_2.

Moreover, the structure with capacitive coupling between the feed line and the resonators is utilized. Then, the ring resonators are directly connected at the corner. The complete width dimensions are W_0 = 2 mm, W_1 = 12.2 mm, W_2 = 4 mm, L_0 = 4.8 mm, L_1 = 6 mm, and L_2 = 12 mm. Then, the proposed BPF is simulated using a Duroid Rogers RT 5880 substrate with ε_r = 2.2, tan δ = 0.0009, and h = 1.575 mm. Parametric iteration is needed to optimize the BPF structure.

Figure 5 shows the parametric iteration of W_1 and its effect on the transmission coefficient or S_{21}. Moreover, Figure 6 shows the parametric iteration of W_1 and its effect on the reflection coefficient or S_{11} of single-band BPF. It can be seen that the width of W_1 is simulated from 10.2 mm to 15.2 mm with a step value of 1.0 mm. The dimension W_1 greatly affects the frequency center shift of BPF. The simulation was carried out between the frequencies of 1.75 GHz to 4.25 GHz. In general, the value of S_{21} at the center frequency has a good value with S_{21}>-3 dB. Meanwhile, the transmission zero value is also around -30 dB.

In addition, the simulation results show that transmission zero occurs at two different frequencies. The reflection coefficient value also has a good value of S_{11}<-10 dB. It shows that the signal is sent properly into the filter device. Moreover, the S_{11} interference is also relatively small. Where the value of S_{11} is around -4 dB, which is at a frequency of 2.75 GHz, in this parameter, the W_1 value of 12.2 mm is most suitable for a single band-band pass filter. The next step is focused on the design of a dual-band band-pass filter based on close-ring resonators.

In detail, the next part is designing a dual-band via-less microstrip band-pass filter based on multi-structure close-ring resonators.

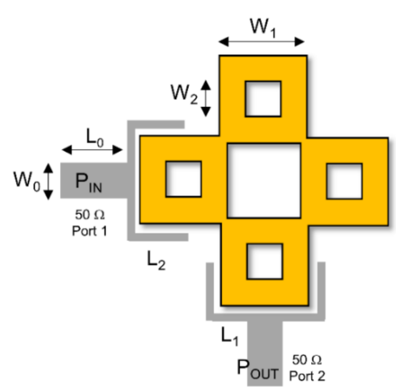

Figure 4. Proposed single band via-less microstrip band-pass filter based on multi-structure close ring resonators.

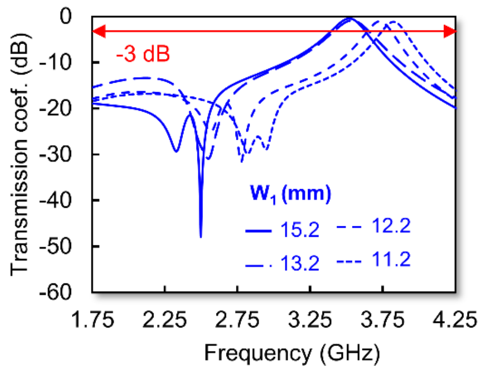

Figure 5. The parametric iteration of W_1 and its effect on the transmission coefficient of single-band BPF.

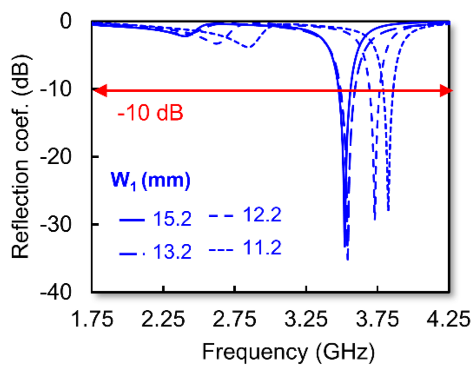

Figure 6. The parametric iteration of W_1 and its effect on the reflection coefficient of single-band BPF.

The overall structure is shown in Figure 7. It can be seen that the dual-band BPF has an additional ring resonator with an outer dimension (W_3) and an inner dimension (W_4). It should be noted that the second resonator can generate the second band at a lower frequency. It means that the total impedance will affect the additional pass band. Moreover, Figure 8 shows the parametric iteration of W_3 and its effect on transmission coefficient value. The simulation was conducted from 1.75 GHz to 4.25 GHz. Then, Figure 9 shows the parametric iteration of W_3 and its effect on the reflection coefficient. The first simulation with $W_3 = 4.2$ mm length obtained a resonance frequency of 2.2 GHz for the first band and 3.4 GHz for the second band. Moreover, it has a value of $S_{11} = -16.9$ dB and $S_{11} = -16.5$ dB for the lower and upper bands. Then, the S_{21} values are -0.89 dB and -1.14 dB for the lower and upper bands.

The next simulation was conducted at $W_3 = 5.2$ mm. It produced 2.3 GHz and 3.6 GHz for the lower and upper bands, respectively. Moreover, the values of S_{11} and S_{21} are -16.4 dB/-9.8 dB and -1.0 dB/-1.6 dB for the upper and lower bands. The following simulation was conducted at $W_3 = 6.2$ mm. It produced 2.17 GHz and 3.7 GHz for the lower and upper bands, respectively.

Moreover, the values of S_{11} and S_{21} are -13.7 dB/-14.4 dB and -0.73 dB/-1.42 dB for the upper band and lower band. Overall, by using $W_3 = 4.2$ mm, the dual-band response was generated. It should be noted that during the iteration process, it is important to consider not only the working frequency value but also the reflection coefficient. In our opinion, the value of $W_3 = 4.2$ serves as a sufficient limit. Moreover, the dimensions of $W_3 = 7.2$ and 8.2 mm are not good due to producing a higher frequency band. In summary, it is crucial to consider all relevant factors and specifications to ensure the desired performance of the resonator.

Then, Figure 10 shows the surface current flows of the proposed single-band BPF. Moreover, Figure 11 and Figure 12 show surface current flows at the proposed dual-band BPF's lower and upper bands, respectively. Based on the simulation, the maximum flows of surface current have a different location for the upper and lower

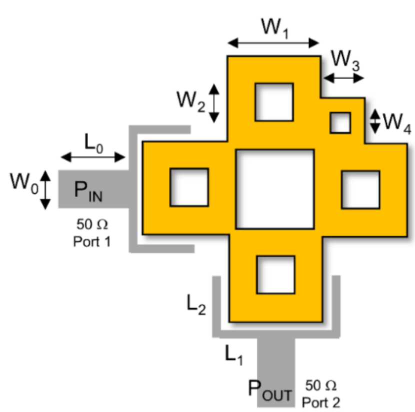

Figure 7. Proposed dual-band via-less microstrip band-pass filter based on multi-structure close ring resonators.

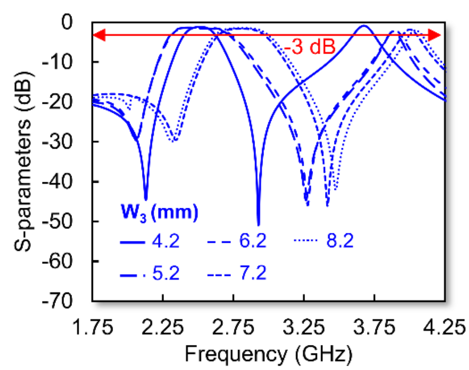

Figure 8. The parametric iteration of W_3 and its effect on the transmission coefficient value of the proposed dual-band BPF.

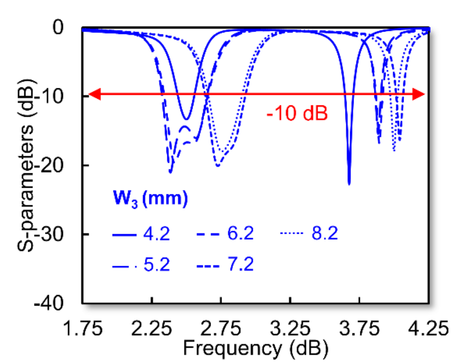

Figure 9. The parametric iteration of W_3 and its effect on the reflection coefficient of the proposed dual-band BPF.

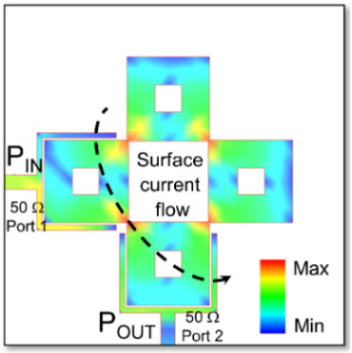

Figure 10. Surface current flows of proposed single band BPF.

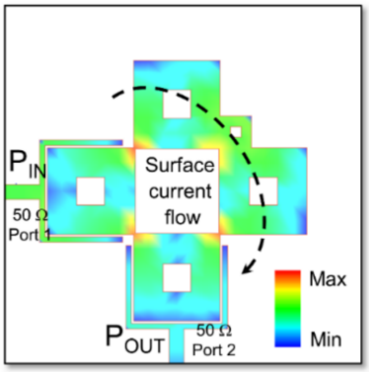

Figure 11. Surface current flows at the lower band of proposed dual band BPF.

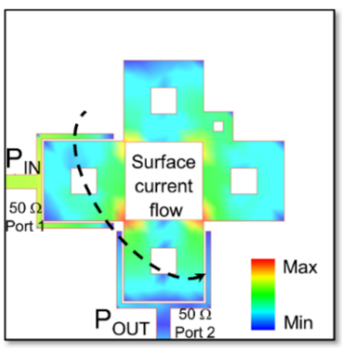

Figure 12. Surface current flows at the upper-band of the proposed dual-band BPF.

bands. Figure 13 and Figure 14 show the fabrication results of the single-band and dual-band BPF, respectively. The realized BPF has a total dimension of 42.3 mm × 42.3 mm. The input connectors and output connectors have a load of 50 ohms.

Figure 15 shows the comparison of S_{21} between the simulation and measurement results. During the simulation, the microstrip single-band BPF operates at a resonant frequency of 3.51 GHz with a value of S_{21} = -0.47 dB. Meanwhile, when taking measurements, this microstrip filter operates at a resonant frequency of 3.53 GHz with a value of S_{21} = -1.03 dB. At the time of measurement, there was an increase in the value of S_{21}, but this situation still resulted in a good value of S_{21} because it was still below -3 dB. Meanwhile, the

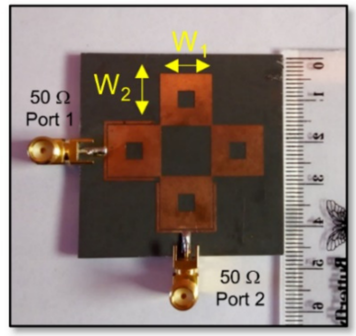

Figure 13. Fabrication of proposed single band via-less microstrip band-pass filter based on multi-structure close ring resonators.

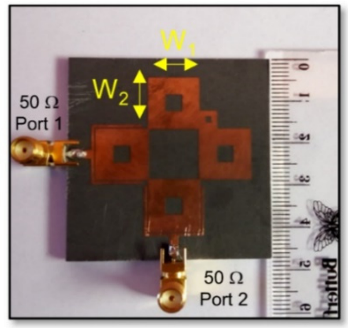

Figure 14. Fabrication of the proposed dual-band via-less microstrip band-pass filter based on multi-structure close ring resonators.

transmission zero value during the simulation reached -40.3 dB. Meanwhile, in one measurement, a value of -30.1 dB was obtained.

Figure 16 compares the S_{11} values from the simulation and measurement results. The simulation results show that the microstrip single-band BPF operates at a resonant frequency of 3.51 GHz with a value of S_{11} = -31.3 dB. Meanwhile, when taking measurements, this microstrip filter operates at a resonant frequency of 3.53 GHz with a value of S_{11} = -34.2 dB. Meanwhile, the bandwidth value during the simulation is 220 MHz, while the measurement is 170 MHz.

Comparison of simulations and measurements shows the measurements and decrease increase in the value of S_{11} = -2.90 dB of simulations. However, this condition is still good because it is below -10 dB. Then, Figure 17 and Figure 18 show a transmission coefficient comparison and reflection coefficient comparison of simulation and measurement of the proposed dual-band via-less microstrip BPF, respectively. Figure 17 shows a comparison of the S_{21} value from the simulation results and the measurement results. During the dual-band BPF simulation in the first band, it operates at a resonant frequency of 2.50 GHz with a value of S_{21} = -1.09 dB, while in the second band, the dual-band BPF operates at a resonant frequency of 3.65 GHz with a value of S_{21} = -0.84 dB.

Based on the measurement results of the first band, the dual-band BPF operates at a resonant frequency of 2.50 GHz with a value of S_{21} = -2.18 dB, while in the second band, a resonant frequency of 3.70 GHz is obtained with a value of S_{21} = -1.43 dB. The bandwidth

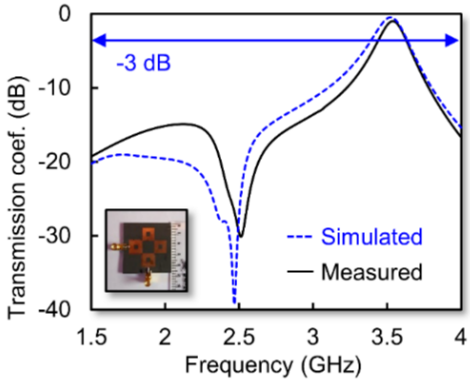

Figure 15. Transmission coefficient comparison of simulation and measurement of proposed single band via-less microstrip BPF.

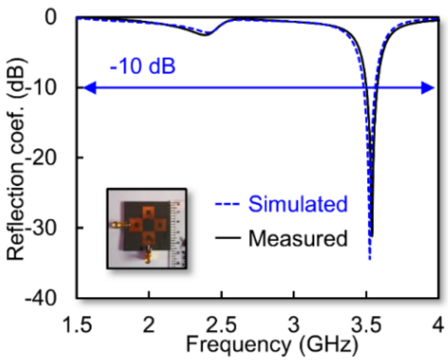

Figure 16. Reflection coefficient comparison of simulation and measurement of proposed single band via-less microstrip BPF.

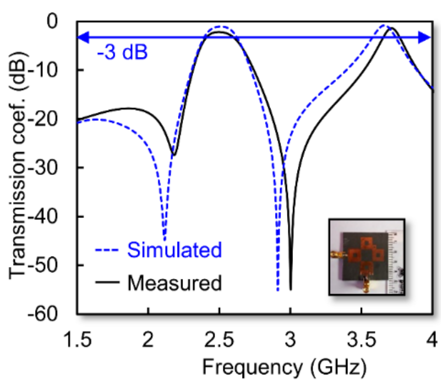

Figure 17. The transmission coefficient comparison of simulation and measurement of proposed dual-band via-less microstrip BPF.

of the microstrip filter frequency during the simulation in the first band is 210 MHz, and in the second band is 150 MHz, while the measurement in the first band is 160 MHz and in the second band is 110 MHz.

Based on the simulation results with measurements on this comparison chart, there is no change in frequency, and it tends to be in a steady state, both from the S_{11} and S_{21} values in the first or second band. Meanwhile, in Figure 18, a comparison graph of S_{11} is obtained from the simulation and S_{11} from the measurement results.

The dual-band BPF simulation in the first band operates at a resonant frequency of 2.5 GHz with a value

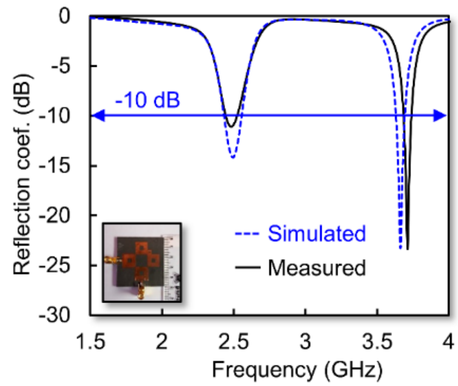

Figure 18. Reflection coefficient comparison of simulation and measurement proposed dual-band via-less microstrip BPF.

of S_{11} = -14.1 dB, while in the second band, the dual-band BPF operates at a resonant frequency of 3.65 GHz with a value of S_{11} = -23.2 dB.

Then, based on the measurement results of the first band, a resonant frequency of 2.5 GHz is obtained with a value of S_{11} = -11.05 dB, while in the second band, a resonant frequency of 3.7 GHz is obtained with a value of S_{11} = -23.3 dB. At the time of measurement, there was a decrease in the S_{11} value, but the S_{11} value was still excellent because it was still below -10 dB.

IV. Conclusion

A dual-band BFP was investigated based on a cascaded closed ring resonator without vias. In detail, the proposed structure consists of several CCRRs connected at the corner part and has a capacitive coupled to the input impedance. Moreover, the CCCR configuration has a different dual size to obtain dual-band performance. Then, the proposed BPF is simulated and fabricated using Duroid Rogers RT 5880 with $\varepsilon_r = 2.2$, tan $\delta = 0.0009$, and h = 1.575 mm. The measurement results demonstrate that the dual-band BPF operates at a resonant frequency of 2.50 GHz with a transmission coefficient (S_{21}) value of -2.18 dB in the first band. In the second band, a resonant frequency of 3.70 GHz is obtained with an S_{21} value of -1.43 dB. The bandwidth in the first band is 160 MHz, and in the second band, it is 110 MHz. Moreover, based on the measurement results, the reflection coefficient (S_{11}) in the first band is -11.05 dB, while in the second band, it is -23.3 dB. The excellent agreement between the simulation and measurement validates the proposed method.

Declarations

Conflict of Interest

The authors have declared that no competing interests exist.

CRediT Authorship Contribution

Teguh Firmansyah: Conceptualization, Methodology Investigation, Writing-Reviewing and Editing; Supriyanto Praptodiyono: Supervision, Funding Acquisition. Achmad Rifai: Conceptualization, Methodology, Software. Syah Alam: Writing-Reviewing and Editing. Ken Paramayudha: Writing-Reviewing and Editing.

Funding

The authors do not receive financial support for the research, authorship, and/or publication of this article.

Acknowledgment

This work was supported by the Kementerian Pendidikan, Kebudayaan, Riset, dan Teknologi Indonesia, fiscal year of 2023.

REFERENCES

[1] Y. S. Mezaal and A. S. Al-Zayed, "Design of microstrip bandpass filters based on stair-step patch resonator," *Int. J. Electron.*, vol. 106, no. 3, pp. 477–490, 2019, doi: 10.1080/00207217.2018.1545144.

[2] Y. I. A. Al-Yasir, N. OjaroudiParchin, A. Abdulkhaleq, K. Hameed, M. Al-Sadoon, and R. Abd-Alhameed, "Design, simulation and implementation of very compact dual-band microstrip bandpass filter for 4G and 5G applications," in *2019 16th Int. Conf. Synth. Model. Anal. Simul. Methods Appl. to Circuit Des.*, 2019, pp. 41–44. doi: 10.1109/SMACD.2019.8795226.

[3] F. Cheng, X. Li, P. Lu, and K. Huang, "A microstrip bandpass filter with 2 independently tunable transmission zeros," *Microw. Opt. Technol. Lett.*, vol. 62, no. 5, pp. 1951–1956, 2020, doi: 10.1002/mop.32275.

[4] X. Wu, M. Nafe, A. A. Melcón, J. S. Gómez-Díaz, and X. Liu, "A non-reciprocal microstrip bandpass filter based on spatio-temporal modulation," in *2019 IEEE Microw. Theory Technol. Soc. Int. Microw. Symp.*, 2019, pp. 9–12. doi: 10.1109/MWSYM.2019.8700732.

[5] C. Luo *et al.*, "Quasi-reflectionless microstrip bandpass filters using bandstop filter for out-of-band improvement," *IEEE Trans. Circuits Syst. II Express Briefs*, vol. 67, no. 10, pp. 1849–1853, 2019, doi: 10.1109/TCSII.2019.2946915.

[6] F. Darwis *et al.*, "Cross-coupled line bandpass filter based on modified parallel-coupled line structure," *Jurnal Elektronika dan Telekomunikasi*, vol. 22, no. 1, pp. 8–13, 2022, doi: 10.55981/jet.474.

[7] R. A. Maulidini, M. R. Hidayat, and T. Praludi, "Band-pass filter microstrip at 3 GHz frequency using square open-loop resonator for S-band radar applications," *Jurnal Elektronika dan Telekomunikasi*, vol. 20, no. 2, pp. 53–59, 2020, doi: 10.14203/jet.v20.53-59.

[8] A. Setiawan *et al.*, "Design and realization of band pass filter in K-band frequency for short range radar application," *Jurnal Elektronika dan Telekomunikasi*, vol. 21, no. 1, pp. 1–7, 2021, doi: 10.14203/jet.v21.1-7.

[9] A. B. Santiko, Y. S. Amrullah, Y. Wahyu, M. I. Maulana, and B. Setia, "Design and realization of coupled line bandpass filter using compact structure at frequencies of 3300 MHz–3400 MHz for Wimax application," *J. Elektron. dan Telekomun.*, vol. 16, no. 1, pp. 11–14, 2016, doi: 10.14203/jet.v16.11-14.

[10] T. Firmansyah *et al.*, "Dual-wideband band pass filter using folded cross-stub stepped impedance resonator," *Microw. Opt. Technol. Lett.*, vol. 59, no. 11, pp. 2929-2934, 2017, doi: 10.1002/mop.30848.

[11] D. Aribowo, Herudin, M. S. B. Haris, and T. Firmansyah, "Design of dual-band bandpass filter based on multistub resonator structure at frequency of 900 MHz and 1.85 GHz," *Int. J. Adv. Trends Comput. Sci. Eng.*, vol. 9, no. 5, 2020, doi: 0.30534/ijatcse/2020/75952020.

[12] T. Firmansyah, Herudin, C. Chairunissa, M. Alaydrus, and G. Wibisono, "Multi-wideband bandpass filter using meandered stub-stepped impedance resonators for multiband application," *Int. J. Commun. Antenna Propag.*, vol. 8, no. 5, pp. 364–373, 2018, doi: 10.15866/irecap.v8i5.14169.

[13] G. Wibisono, Yudiansyah, and T. Firmansyah, "Compact quad-wideband BPF based on dual-stub step impedance resonator with meandering structure," in *IEEE Reg. 10 Annu. Int. Conf. Proc.*, 2019, doi: 10.1109/TENCON.2018.8650111.

[14] T. Firmansyah, S. Praptodiyono, A. S. Pramudyo, C. Chairunissa, and M. Alaydrus, "Hepta-band bandpass filter based on folded cross-loaded stepped impedance resonator," *Electron. Lett.*, vol. 53, no. 16, pp. 1119-1121, 2017, doi: 10.1049/el.2017.1121.

[15] M.-H. Weng, S.-K. Liu, H.-W. Wu, and C.-H. Hung, "A dual-band bandpass filter having wide and narrow bands simultaneously using multilayered stepped impedance resonators," *Prog. Electromagn. Res. Lett.*, vol. 13, pp. 139–147, 2010, doi: 10.2528/PIERL10022401.

[16] H. Chang, W. Sheng, J. Cui, and J. Lu, "Multilayer dual-band bandpass filter with multiple transmission zeros using discriminating coupling," *IEEE Microw. Wirel. Components Lett.*, vol. 30, no. 7, pp. 645–648, 2020, doi: 10.1109/LMWC.2020.2995181.

[17] H. H. Ta and A.-V. Pham, "Dual band band-pass filter with wide stopband on multilayer organic substrate," *IEEE Microw. Wirel. components Lett.*, vol. 23, no. 4, pp. 193–195, 2013, doi: 10.1109/LMWC.2013.2251617.

[18] A. M. Elelimy and A. M. El-Tager, "Dual-band BPF embedded in multilayer low temperature co-fired ceramics (LTCC) for Wimax applications," in *2014 Int. Conf. Eng. Technol.*, 2014, doi: 10.1109/ICEngTechnol.2014.7016777.

[19] D. Tang, C. Han, Z. Deng, H. J. Qian, and X. Luo, "Substrate-integrated defected ground structure for single- and dual-band bandpass filters with wide stopband and low radiation loss," *IEEE Trans. Microw. Theory Tech.*, vol. 69, no. 1, pp. 659–670, 2020, doi: 10.1109/TMTT.2020.3038202.

[20] S. Zhang, J.-Y. Rao, J.-S. Hong, and F.-L. Liu, "A novel dual-band controllable bandpass filter based on fan-shaped substrate integrated waveguide," *IEEE Microw. Wirel. Components Lett.*, vol. 28, no. 4, pp. 308–310, 2018, doi: 10.1109/LMWC.2018.2805460.

[21] A. Iqbal, J. J. Tiang, C. K. Lee, N. K. Mallat, and S. W. Wong, "Dual-band half mode substrate integrated waveguide filter with independently tunable bands," *IEEE Trans. Circuits Syst. II Express Briefs*, vol. 67, no. 2, pp. 285–289, 2019, doi: 10.1109/TCSII.2019.2911014.

[22] Z. Ruan, D. Shen, H. Yuan, and X. Zhang, "A self-packaged ultra-wide band bandpass filter using integrated substrate gap waveguide," in *2019 IEEE Microw. Theory Technol. Soc. Int. Wirel. Symp.*, 2019, doi: 10.1109/IEEE-IWS.2019.8804146.